Gust Velocity Spatial Distribution Effects on Lateral-Directional Response of VTOL Aircraft

ROBERT L. SWAIM* AND ALONZO J. CONNORS†
Air Force Flight Dynamics Laboratory, Wright-Patterson Air Force Base, Ohio

The effects of spanwise distribution of longitudinal and vertical components of gust velocity and longitudinal distribution of the lateral component on the lateral-directional response of a nearly hovering VTOL aircraft are analyzed. Results show that spanwise effects of the longitudinal and vertical components are negligible, and the longitudinal distribution of the lateral component is significant in computing the power spectral densities of gust-induced side force, yawing moment, rolling moment, and the aircraft sideslip, yaw, and roll rms response angles. If the gust-induced angles of attack and sideslip angles are in the nonlinear range of lift curve slope, the foregoing conclusions, which are based on linear aerodynamic theory, may not hold, and an analysis based on momentum transfer of gust energy to the aircraft is recommended.

Nomenclature

b = wing span
$C_{L\alpha}$ = wing lift curve slope
$C_{l\beta}$ = rolling moment due to sideslip stability derivative
C_{l_p} = rolling moment due to rolling velocity stability derivative
C_{l_r} = rolling moment due to yawing velocity stability derivative
$C_{n\beta}$ = yawing moment due to sideslip stability derivative
C_{n_p} = yawing moment due to rolling velocity stability derivative
C_{n_r} = yawing moment due to yawing velocity stability derivative
$C_{y\beta}$ = side force due to sideslip stability derivative
C_{y_p} = side force due to rolling velocity stability derivative
C_{y_r} = side force due to yawing velocity stability derivative
$D\phi_g$, $D\psi_g$ = equivalent rolling and yawing gust gradients
g = acceleration of gravity
I_x, I_z, I_{xz} = moments and product of inertia
j = $(-1)^{1/2}$
L, N, Y = gust-induced rolling moment, yawing moment, and side force, respectively
L' = integral scale of turbulence
L_p = $\rho U_0 S b^2 C_{l_p}/4I_x$
L_r = $\rho U_0 S b^2 C_{l_r}/4I_x$
L_v = $\rho U_0 S b C_{l\beta}/2I_x$
$l(u_g)$ = local wing section lift due to u_g
$l(w_g)$ = local wing section lift due to w_g
M = airplane mass
N_p = $\rho U_0 S b^2 C_{n_p}/4I_z$
N_r = $\rho U_0 S b^2 C_{n_r}/4I_z$
N_v = $\rho U_0 S b C_{n\beta}/2I_z$
$N_{\dot{v}}$ = $\rho U_0 S b C_{n\dot{\beta}}/2I_z$
p, r = rolling and yawing velocities
S = planform reference area
s = Laplace transform complex variable
U, V, W = orthogonal components of total relative wind velocity
u_g, v_g, w_g = orthogonal gust velocity components
Y_p = $\rho U_0 S b C_{y_p}/4M$
Y_r = $\rho U_0 S b C_{y_r}/4M$
Y_v = $\rho U_0 S C_{y\beta}/2M$
α, β, θ = perturbation angles of attack, sideslip, and pitch
α_0 = steady-state or trim angle of attack
β_g = gust-induced sideslip angle
γ_0 = trim flightpath angle
ρ = freestream air density
σ_{u_g}, σ_{v_g}, σ_{w_g} = rms values of gust velocity components
σ_β, σ_ψ, σ_ϕ = rms values of sideslip, yaw, and roll response angles
$\Phi_{D\phi_g}$, $\Phi_{D\psi_g}$ = power spectral densities of equivalent rolling and yawing gust gradients
$\Phi_{L(w_g)}$, $\Phi_{N(w_g)}$ = power spectral densities of w_g-induced rolling and yawing moments
$\Phi_{L(u_g)}$, $\Phi_{N(u_g)}$ = power spectral densities of u_g-induced rolling and yawing moments
$\Phi_{Y(v_g)}$ = power spectral density of v_g-induced side force
Φ_{u_g}, Φ_{v_g}, Φ_{w_g} = power spectral densities of gust velocity components
Φ_β, Φ_ψ, Φ_ϕ = power spectral densities of sideslip, yaw, and roll response angles
ϕ, ψ = perturbation roll and yaw response angles

Subscripts

W = effect due to the wing
T = effect due to the vertical tail
WT = effect due to the wing and vertical tail
FT = effect due to the fuselage and vertical tail
0 = steady-state, mean, or trim value

Received March 29, 1967; revision received October 4, 1967. This research was conducted internally under Air Force sponsorship. This article may be reproduced for any use of the U.S. Government. Distribution is unlimited.

* Senior Research Engineer; now Associate Professor of Aeronautics, Astronautics, & Engineering Sciences, Purdue University, Lafayette, Ind. Associate Fellow AIAA.
† Mathematician.

Introduction

THE design of flight control systems for VTOL aircraft is still very much an art rather than a well-defined and documented procedure. Attempts to apply to VTOL design analytical approaches which were developed for conventional types of aircraft have had only limited success in many cases. One such area of limited success is in analytically modeling and analyzing the dynamic response to atmospheric turbulence during hover and transition flight. A fundamental difficulty in this case involves providing a valid analytical representation of the turbulence-generated disturbance forces and moments acting on the aircraft.

The sources of aerodynamic forces and moments acting on VTOL aircraft in low-altitude hover or near-hover flight modes are the three orthogonal components of wind relative velocity, U, V, and W, where, in general, each contains a mean or steady relative wind component U_0, V_0, and W_0 and turbulence or gust components u_g, v_g, and w_g. For purposes of point stability or frozen point dynamic analysis, the air-

craft is usually assumed headed into the mean wind. In this case,

$$U = U_0 + u_g \qquad V = v_g \qquad W = w_g$$

u_g, v_g, and w_g will create forces and moments on the aircraft by primarily two mechanisms: 1) circulation lift due to Bernoulli's theorem and the Kutta-Joukowsky law of circulation, and 2) momentum transfer between the gust velocity components and the airframe.

For conventional aircraft, where the flight speed is essentially U_0 and $U_0 \gg u_g$, v_g, w_g, V_0, W_0, the gust aerodynamic forces and moments (other than drag) are largely due to circulation lift. However, as a VTOL aircraft transitions to hovering flight, the contribution due to circulation decreases to the point where it may well be of the same order of magnitude as the contribution due to momentum transfer when turbulence is severe. Therefore, a valid aerodynamic theory in the hovering mode must account for both types of inputs.

Circulation lift theories are well-developed for conventional aircraft and express the results in Taylor series expansions (based on small perturbations) involving coefficients and stability derivatives. Such theories are not nearly as accurate for VTOL hover due to violation of the small angle assumption on gust inputs—that is, inputs in the nonlinear range of the lift curve slope. There are no good aerodynamic theories which adequately describe the gust input forces and moments due to either circulation or momentum transfer, let alone both simultaneously, for VTOL vehicles in or near hover. Consequently, VTOL designers continue to use the stability derivative approach for describing vehicle gust input forces in hover even though the applicability is questionable in many cases. It should be pointed out, however, that it is still probably accurate enough to use a Taylor series expansion (with stability derivatives) of the aerodynamic forces and moments resulting from the motions of the aircraft. These motions are likely to be within the small-perturbation assumption on the dependent variables such as pitch angle θ, angle of attack α, etc.—particularly where the VTOL vehicle has a stability augmentation system (as most do), which tends to maintain small angle responses to gusts and other disturbances.

A further complication in computing the gust forces and moments occurs when one wishes to account for the effects of distributed gust velocities along the fuselage (penetration effects) and across the wing span. For example, variations in longitudinal component u_g and vertical component w_g across the wing span at any time instant will induce rolling and yawing moments, as will variations in lateral component v_g along the fuselage. The objective of the research reported herein was to determine the importance of these gust velocity distributions on the lateral-directional response of hovering VTOL aircraft.

The approach taken, using power spectral density analytical techniques, was to compare the vehicle yaw, roll, and sideslip angle responses with and without the velocity distribution effects being accounted for. The critical factor was in the mathematical method used to describe the gust input forces and moments. To the authors' knowledge, only two methods are available and both were developed for application to aircraft in conventional flight, where the flight velocity is much larger than the gust component velocities. This assures that the gust-induced forces and moments are due largely to circulation lift, with negligible momentum transfer between gust field and aircraft. The first method[1] uses aerodynamic transfer functions to describe the gust input forces and moments. This method requires considerably more information on the aerodynamic characteristics of the aircraft in the form of frequency response functions than does the second method. For this reason the second method[2] was used to describe the gust-induced forces and moments acting on the hovering aircraft. In this method the gust velocities are represented as equivalent rigid-body rotations of the airplane; namely, rolling gusts, yawing gusts, and side gusts. The random distributions of gust velocities across the span and the fuselage penetration effects are accounted for in defining the rolling, yawing, and side gusts. Flowfield interaction effects due to lift engine exhaust were neglected, though these would be important in a quantitative design.

Equations of Motion

The three-degree-of-freedom, lateral-directional, small-perturbation equations of motion of a free airframe can be written as in Eq. (1)[3]:

$$\begin{bmatrix} MU_0(s - Y_v) & -MY_r s - Mg\sin\gamma_0 & M(-Y_p s - g\cos\gamma_0) \\ -I_z U_0(N_v' s + N_v) & I_z(s^2 - N_r' s) & -I_{xz}s^2 - I_z N_p' s \\ -I_x U_0 L_v' & -I_{xz}s^2 - I_x L_r' s & I_x(s^2 - L_p' s) \end{bmatrix} \begin{bmatrix} \beta \\ \psi \\ \phi \end{bmatrix} = \begin{bmatrix} Y \\ N \\ L \end{bmatrix} \tag{1}$$

β, ψ, and ϕ are the small-perturbation sideslip, yaw, and roll angles, respectively. Y, N, and L are the respective side force, yawing moment, and rolling moment induced by the three components of gust velocity u_g, v_g, and w_g.

In order to simplify the description of Y, N, and L, it has been assumed that the side force Y is due to v_g acting on the fuselage and vertical tail, the yawing moment N is due to u_g and w_g acting on the wing and v_g acting on the fuselage and vertical tail, and the rolling moment L is due to u_g, v_g, and w_g acting on the wing and v_g acting on the vertical tail. Thus,

$$Y = Y_{FT}(v_g) \qquad N = N_W(u_g, w_g) + N_{FT}(v_g)$$
$$L = L_W(u_g, v_g, w_g) + L_T(v_g)$$

Or, in matrix transfer function form,

$$\begin{bmatrix} Y \\ N \\ L \end{bmatrix} = \begin{bmatrix} 0 & \left(\frac{Y}{v_g}\right)_{FT} & 0 \\ \left(\frac{N}{u_g}\right)_W & \left(\frac{N}{v_g}\right)_{FT} & \left(\frac{N}{w_g}\right)_W \\ \left(\frac{L}{u_g}\right)_W & \left\{\left(\frac{L}{v_g}\right)_W + \left(\frac{L}{v_g}\right)_T\right\} & \left(\frac{L}{w_g}\right)_W \end{bmatrix} \begin{bmatrix} u_g \\ v_g \\ w_g \end{bmatrix} \tag{2}$$

Denoting the square matrix in Eq. (1) by $D(s)$, we have

$$\begin{bmatrix} \beta \\ \psi \\ \phi \end{bmatrix} = [D(s)]^{-1} \begin{bmatrix} Y \\ N \\ L \end{bmatrix} = \begin{bmatrix} \left(\frac{\beta}{Y}\right) & \left(\frac{\beta}{N}\right) & \left(\frac{\beta}{L}\right) \\ \left(\frac{\psi}{Y}\right) & \left(\frac{\psi}{N}\right) & \left(\frac{\psi}{L}\right) \\ \left(\frac{\phi}{Y}\right) & \left(\frac{\phi}{N}\right) & \left(\frac{\phi}{L}\right) \end{bmatrix} \begin{bmatrix} Y \\ N \\ L \end{bmatrix} \tag{3}$$

Combining Eqs. (2) and (3) gives the matrix equation in Eq. (4). In terms of power spectral densities and assuming

u_g, v_g, and w_g are uncorrelated, we have

$$\begin{bmatrix}\beta\\ \psi\\ \phi\end{bmatrix} = \begin{bmatrix} \left\{\left(\frac{\beta}{N}\right)\left(\frac{N}{u_g}\right)_W + \left(\frac{\beta}{L}\right)\left(\frac{L}{u_g}\right)_W\right\} & \left\{\left(\frac{\beta}{Y}\right)\left(\frac{Y}{v_g}\right)_{FT} + \left(\frac{\beta}{N}\right)\left(\frac{N}{v_g}\right)_{FT} + \left(\frac{\beta}{L}\right)\left[\left(\frac{L}{v_g}\right)_W + \left(\frac{L}{v_g}\right)_T\right]\right\} & \left\{\left(\frac{\beta}{N}\right)\left(\frac{N}{w_g}\right)_W + \left(\frac{\beta}{L}\right)\left(\frac{L}{w_g}\right)_W\right\} \\ \left\{\left(\frac{\psi}{N}\right)\left(\frac{N}{u_g}\right)_W + \left(\frac{\psi}{L}\right)\left(\frac{L}{u_g}\right)_W\right\} & \left\{\left(\frac{\psi}{Y}\right)\left(\frac{Y}{v_g}\right)_{FT} + \left(\frac{\psi}{N}\right)\left(\frac{N}{v_g}\right)_{FT} + \left(\frac{\psi}{L}\right)\left[\left(\frac{L}{v_g}\right)_W + \left(\frac{L}{v_g}\right)_T\right]\right\} & \left\{\left(\frac{\psi}{N}\right)\left(\frac{N}{w_g}\right)_W + \left(\frac{\psi}{L}\right)\left(\frac{L}{w_g}\right)_W\right\} \\ \left\{\left(\frac{\phi}{N}\right)\left(\frac{N}{u_g}\right)_W + \left(\frac{\phi}{L}\right)\left(\frac{L}{u_g}\right)_W\right\} & \left\{\left(\frac{\phi}{Y}\right)\left(\frac{Y}{v_g}\right)_{FT} + \left(\frac{\phi}{N}\right)\left(\frac{N}{v_g}\right)_{FT} + \left(\frac{\phi}{L}\right)\left[\left(\frac{L}{v_g}\right)_W + \left(\frac{L}{v_g}\right)_T\right]\right\} & \left\{\left(\frac{\phi}{N}\right)\left(\frac{N}{w_g}\right)_W + \left(\frac{\phi}{L}\right)\left(\frac{L}{w_g}\right)_W\right\} \end{bmatrix} \begin{bmatrix}u_g\\ v_g\\ w_g\end{bmatrix} = [a_{ij}]\begin{bmatrix}u_g\\ v_g\\ w_g\end{bmatrix} \quad (4)$$

$$\Phi_\beta(\omega) = |a_{11}(\omega)|^2\Phi_{u_g}(\omega) + |a_{12}(\omega)|^2\Phi_{v_g}(\omega) + |a_{13}(\omega)|^2\Phi_{w_g}(\omega) \quad (5)$$

$$\Phi_\psi(\omega) = |a_{21}(\omega)|^2\Phi_{u_g}(\omega) + |a_{22}(\omega)|^2\Phi_{v_g}(\omega) + |a_{23}(\omega)|^2\Phi_{w_g}(\omega) \quad (6)$$

$$\Phi_\phi(\omega) = |a_{31}(\omega)|^2\Phi_{u_g}(\omega) + |a_{32}(\omega)|^2\Phi_{v_g}(\omega) + |a_{33}(\omega)|^2\Phi_{w_g}(\omega) \quad (7)$$

The infinite integrals of Eqs. (5–7) yield the variances or mean square values of the aircraft response angles β, ψ, and ϕ:

$$\sigma_\beta^2 = \int_{-\infty}^{\infty}\Phi_\beta(\omega)d\omega \quad (8)$$

$$\sigma_\psi^2 = \int_{-\infty}^{\infty}\Phi_\psi(\omega)d\omega \quad (9)$$

$$\sigma_\phi^2 = \int_{-\infty}^{\infty}\Phi_\phi(\omega)d\omega \quad (10)$$

In order to assess the importance of spanwise and axial (penetration effects) distributions of gust velocities on hovering VTOL aircraft, Eqs. (8–10) were evaluated for a hovering VJ-101, both with and without distribution effects included. From this analysis of a single configuration it was possible to draw some general conclusions.

The a_{ij} matrix in Eq. (4) relates the response angles to the component gust velocities. The elements of a_{ij}, as a function of frequency, are dependent on the airframe transfer functions of Eq. (3) and the gust input transfer functions of Eq. (2). The distribution effects are included in the gust transfer functions.

The flight condition analyzed was that of near-hover over a spot at 50 ft altitude and headed into a 25-fps mean wind. The data used in evaluating the elements of Eq. (1) are: $U_0 = 25$ fps; $\gamma_0 = 5.5°$; $g = 32.2$ ft/sec^2; $M = 471.8$ slugs; $I_x = 18{,}530$ slug-ft^2; $I_z = 45{,}700$ slug-ft^2; $I_{xz} = 5200$ slug-ft^2; $Y_v = -0.034$; $\alpha_0 = -7.5°$; $L_v = -0.00384$; $N_v = 0.000863$; $N_\dot{v} = 0$; $Y_r = 0.106$; $L_r = 0.0109$; $N_r = -0.0228$; $Y_p = -0.0182$; $L_p = -0.0131$; $N_p = -0.00268$. With the substitution of $s = j\omega$, the nine airframe transfer functions of Eq. (3) were determined as a function of ω from Eq. (1). The denominator for each of these nine is

$$\Delta(s) = s(s + 0.0213)(s + 0.507)(s^2 - 0.458s + 0.233) \quad (11)$$

The negative damping in the quadratic factor indicates that the vehicle is unstable and would require stabilization by a stability augmentation system and/or a pilot in the control loop. Without getting into a discussion of what constitutes desirable handling qualities, it was assumed augmentation could be provided which would yield the following closed-loop characteristic polynomial:

$$\bar{\Delta}(s) = (s + 0.1)(s + 0.2)(s + 0.3)(s^2 + 0.2s + 1) \quad (12)$$

This could be achieved using state variable synthesis techniques and sensing of the three outputs ϕ, ψ, and β. In Eq. (12) the dutch-roll quadratic has a damping ratio of 0.1 and natural frequency of 1. rad/sec. In the frequency domain,

$$\frac{\Delta(\omega)}{\bar{\Delta}(\omega)} = \frac{(0.0705\omega^4 - 0.117\omega^2) + j(\omega^5 - 0.0014\omega^3 + 0.0025\omega)}{(0.8\omega^4 - 0.628\omega^2 + 0.006) + j(\omega^5 - 1.23\omega^3 + 0.1112\omega)} \quad (13)$$

The products of Eq. (13) and each of the airframe transfer functions of Eq. (3) give the closed-loop airframe transfer functions. These are used in the evaluation of the a_{ij} matrix of Eq. (4).

Gust-Induced Forces and Moments

Following the method in Refs. 2 and 4 of representing the gust velocities as equivalent rigid-body rotations, consider

$$L(w_g) = -\frac{1}{2}\rho U_0^2 Sb(C_{l_p})_W\frac{p_g b}{2U_0} = \frac{1}{4}\rho U_0^2 Sb(C_{l_p})_W D\phi_g \quad (14)$$

$$L(u_g) = -\frac{1}{2}\rho U_0^2 Sb(C_{l_r})_W\frac{r_g b}{2U_0} = \frac{1}{4}\rho U_0^2 Sb(C_{l_r})_W D\psi_g \quad (15)$$

At any instant, the random distribution of vertical gust velocity w_g across the span has some equivalent average linear spanwise gradient which produces the wing rolling moment $L(w_g)$. $D\phi_g$ as defined by Eq. (14) is the equivalent rolling gust gradient. Likewise, $D\psi_g$ is the equivalent yawing gust gradient due to spanwise distribution of u_g. w_g also produces a wing yawing moment which is assumed to be in phase with the rolling moment (see Ref. 4 for justification). Likewise, u_g produces a wing yawing moment. Thus,

$$N(w_g) = (C_{n_p}/C_{l_p})_W L(w_g) = \tfrac{1}{4}\rho U_0^2 Sb(C_{n_p})_W D\phi_g \quad (16)$$

$$N(u_g) = (C_{n_r}/C_{l_r})_W L(u_g) = \tfrac{1}{4}\rho U_0^2 Sb(C_{n_r})_W D\psi_g \quad (17)$$

The turbulence is assumed to be homogeneous and isotropic. Also, the statistical properties of the gust patches are assumed constant as they traverse the aircraft (Taylor's hypothesis). u_g, v_g, and w_g are assumed to have the following

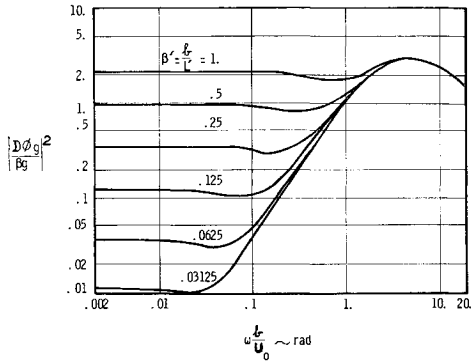

Fig. 1 Ratio of rolling gust to side gust spectra.

power spectral densities:

$$\Phi_{u_g} = \frac{\sigma_{u_g}^2 L'}{\pi U_0} \frac{1}{1 + (\omega L'/U_0)^2} \tag{18}$$

$$\Phi_{v_g} = U_0^2 \Phi_{\beta_g} = \Phi_{w_g} = \frac{\sigma_{v_g}^2 L'}{2\pi U_0} \frac{1 + 3(\omega L'/U_0)^2}{[1 + (\omega L'/U_0)^2]^2} \tag{19}$$

where $\sigma_{u_g}^2 = \sigma_{v_g}^2 = \sigma_{w_g}^2$ and

$$\sigma_{u_g}^2 = \int_{-\infty}^{\infty} \Phi_{u_g} d\omega = \int_{-\infty}^{\infty} \Phi_{v_g} d\omega = \int_{-\infty}^{\infty} \Phi_{w_g} d\omega$$

There is room for argument as to whether or not this mathematical model accurately represents low-altitude turbulence—particularly since such turbulence is not strictly isotropic; however, the model is sufficiently accurate for our purposes here.

Now,

$$\Phi_{D\phi_g} = \left|\frac{D\phi_g}{\beta_g}\right|^2 \Phi_{\beta_g} = \left|\frac{D\phi_g}{\beta_g}\right|^2 \frac{\Phi_{w_g}}{U_0^2} \tag{20}$$

and

$$\Phi_{D\psi_g} = \left|\frac{D\psi_g}{\beta_g}\right|^2 \Phi_{\beta_g} = \left|\frac{D\psi_g}{\beta_g}\right|^2 \frac{\Phi_{w_g}}{U_0^2} \tag{21}$$

Thus, from Eqs. (14) and (15),

$$\Phi_{L(w_g)} = \frac{[\frac{1}{4}\rho U_0^2 Sb(C_{l_p})_W]^2}{U_0^2} \left|\frac{D\phi_g}{\beta_g}\right|^2 \Phi_{w_g} \tag{22}$$

$$\Phi_{L(u_g)} = \frac{[\frac{1}{4}\rho U_0^2 Sb(C_{l_r})_W]^2}{U_0^2} \left|\frac{D\psi_g}{\beta_g}\right|^2 \Phi_{w_g} \tag{23}$$

And from Eqs. (16) and (17),

$$\Phi_{N(w_g)} = (C_{n_p}/C_{l_p})_W^2 \Phi_{L(w_g)} \tag{24}$$

$$\Phi_{N(u_g)} = (C_{n_r}/C_{l_r})_W^2 \Phi_{L(u_g)} \tag{25}$$

$|D\phi_g/\beta_g|^2$ and $|D\psi_g/\beta_g|^2$ are obtained from Figs. 15 and 16

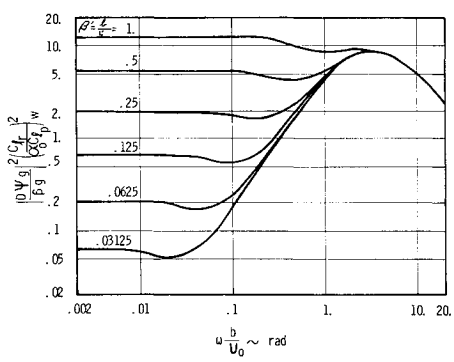

Fig. 2 Ratio of yawing gust to side gust spectra.

of Ref. 2, which are reproduced here as Figs. 1 and 2. The details of the derivations of these curves are given in Refs. 2 and 4 and will not be repeated here. A few words concerning the assumptions made are in order, however. The theory used assumes that the aerodynamic forces vary linearly with u_g and w_g. This implies that u_g and w_g must be sufficiently small compared to the mean wind U_0. The lift curve slopes of most subsonic wings are linear up to about 14° angle of attack. Therefore, since the gust-induced angle of attack is given by $\alpha_g = \arctan w_g/U_0 \cong w_g/U_0$, for a mean wind of 25 fps, we must have $w_g \leq 6$ fps, approximately, for low trim angles of attack. For gust velocities larger than this, the assumption of linear aerodynamics is less valid and momentum transfer of gust energy to the aircraft becomes significant compared to forces due to circulation lift. A further assumption of the linear theory on which Figs. 1 and 2 are based is that the ratio of wing lift due to u_g and wing lift due to w_g is given by[4]

$$l(u_g)/l(w_g) = 2\alpha_0(u_g/w_g) \tag{26}$$

We have

$$l(u_g) = \tfrac{1}{2}\rho[(U_0 + u_g)^2 - U_0^2]SC_{L\alpha}\alpha_0 \tag{27}$$

$$l(w_g) = \tfrac{1}{2}\rho U_0^2 SC_{L\alpha}[\arctan(w_g/U_0)] \tag{28}$$

$$\frac{l(u_g)}{l(w_g)} = \frac{(u_g^2 + 2U_0 u_g)\alpha_0}{U_0^2 \arctan(w_g/U_0)} \tag{29}$$

Comparison of Eqs. (26) and (29) shows they are nearly equal if $u_g \ll U_0$ and $w_g \ll U_0$. If $u_g = w_g = 6$ fps, then Eq. (29) gives $l(u_g)/l(w_g) = 2.24\ \alpha_0$, compared to $2\alpha_0$ from Eq. (26)—about a 10% error. With the limit of about 6 fps on u_g and w_g magnitudes, the aerodynamic theory used is reasonably accurate in accounting for the gust forces acting on the aircraft hovering in a 25-fps mean wind at low angles of attack. And in fact, reasonably good representation can be expected as long as the ratios of component gust velocities to mean wind velocity are less than about 6/25.

Consider now the effects of the lateral gust velocity component v_g. The yawing moment of the fuselage and vertical tail, due to penetration into lateral gusts referenced at the center of gravity, has been derived in Ref. 5, where a simple profile shape was used to define the side force distribution over the fuselage and vertical tail due to sinusoidal v_g components. As developed in Ref. 5 and summarized in Ref. 2,

$$\left(\frac{N}{v_g}\right)_{FT} = \pi\rho U_0 \left\{ \frac{-2x_0 s_0^2}{k_0^3} [(2k_0 - jk_0^2 + j2)e^{jk_0} - j2] + \frac{(x_2 - x_1)(s_1 - s_0)^2}{(k_2 - k_1)^3} [(2k_2 - k_1 - j2 - jk_1k_2 + jk_2^2)e^{-jk_2} - (k_1 - j2)e^{-jk_1}] \right\} \tag{30}$$

where $k_n = \omega x_n/U_0$, $(n = 0, 1, 2)$; and x_0, x_1, x_2, s_0, and s_1 are the profile dimensions shown in Fig. 3. Equation (30) is based on slender-body theory and requires small sideslip angles; again $v_g/U_0 = 6/25$ gives about 10% error. The side force transfer function is given in Eq. (31):

$$\left(\frac{Y}{v_g}\right)_{FT} = \pi\rho U_0 \left\{ \frac{2s_0^2}{k_0^2} [1 - (1 - jk_0)e^{jk_0}] + \left(\frac{s_1 - s_0}{k_2 - k_1}\right)^2 [e^{-jk_1} - (1 - jk_1 + jk_2)e^{-jk_2}] \right\} \tag{31}$$

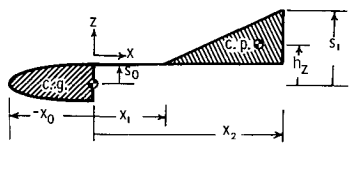

Fig. 3 Fuselage profile.

Now, at $\omega = 0$ it can be shown that Eqs. (30) and (31) reduce to

$$\left(\frac{N}{v_g}\right)_{FT} = \frac{\pi\rho U_0}{3}\left[-2s_0^2x_0 + (s_1 - s_0)^2\left(x_2 + \frac{x_1}{2}\right)\right] = \frac{1}{2}\rho U_0 Sb(C_{n\beta})_{FT} \quad (32)$$

$$\left(\frac{Y}{v_g}\right)_{FT} = \frac{-\pi\rho U_0}{2}[2s_0^2 + (s_1 - s_0)^2] = \frac{1}{2}\rho U_0 S(C_{y\beta})_{FT} \quad (33)$$

$(C_{n\beta})_{FT}$ and $(C_{y\beta})_{FT}$ are fuselage-tail steady-state stability derivatives, and the profile parameters in Fig. 3 should be adjusted so that Eqs. (32) and (33) are satisfied.

The rolling moment transfer function due to lateral gusts on the wing and vertical tail is

$$(L/v_g)_{WT} = (L/v_g)_W + (L/v_g)_T \quad (34)$$

where

$$(L/v_g)_W = \tfrac{1}{2}\rho U_0 Sb(C_{l\beta})_W \quad (35)$$

As derived in Ref. 5, the second term in Eq. (31) is the side force due to the vertical tail. Thus,

$$\left(\frac{L}{v_g}\right)_T = \pi\rho U_0 h_z\left(\frac{s_1 - s_0}{k_2 - k_1}\right)^2[e^{-jk_1} - (1 - jk_1 + jk_2)e^{-jk_2}] \quad (36)$$

where h_z is the distance of the vertical tail profile center of pressure above the x axis. At $\omega = 0$, it can be shown that Eq. (36) reduces to

$$(L/v_g)_T = -\tfrac{1}{2}\pi\rho U_0 h_z(s_1 - s_0)^2 = \tfrac{1}{2}\rho U_0 Sb(C_{l\beta})_T \quad (37)$$

where $(C_{l\beta})_T$ is the vertical tail rolling moment due to sideslip steady-state stability derivative. h_z must be chosen so that Eq. (37) is satisfied. Thus,

$$h_z = [-Sb(C_{l\beta})_T]/\pi(s_1 - s_0)^2 \quad (38)$$

Combining Eqs. (34–36 and 38) gives

$$(L/v_g)_{WT} = (L/v_g)_W + (L/v_g)_T = \frac{-\rho U_0 Sb(C_{l\beta})_T}{(k_2 - k_1)^2}[e^{-jk_1} - (1 - jk_1 + jk_2)e^{-jk_2}] + \frac{1}{2}\rho U_0 Sb(C_{l\beta})_W \quad (39)$$

For the VJ-101 aircraft and flight condition analyzed herein, the steady-state stability derivatives and profile

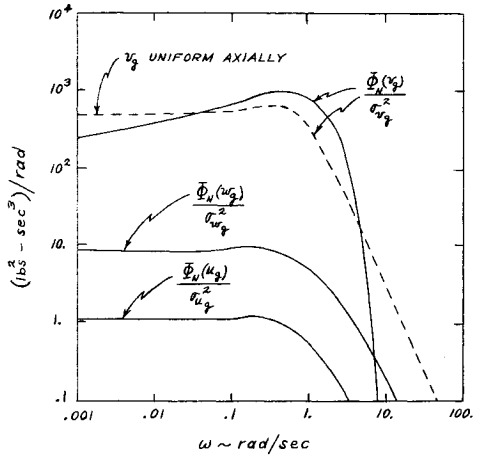

Fig. 4 Yawing moment power spectra.

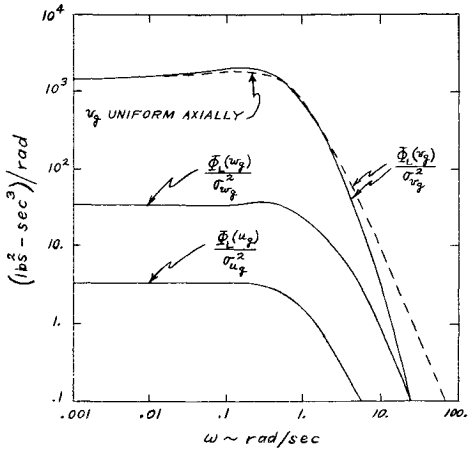

Fig. 5 Rolling moment power spectra.

parameters needed in the foregoing equations are tabulated below:

$(C_{l\beta})_W = -0.3$	$(C_{y\beta})_{FT} = -2.711$	$x_1 = -18$ ft	
$(C_{l\beta})_T = -0.307$	$(C_{n\beta})_{FT} = 0.337$	$x_2 = 16$ ft	
$(C_{l_r})_W = 0.175$	$b = 19.69$ ft	$k_0 = 0.96\omega$ rad	
$(C_{l_p})_W = -0.21$	$S = 200$ ft^2	$k_1 = -0.72\omega$ rad	
$(C_{y\beta})_T = -2.43$	$s_0 = 3$ ft	$k_2 = 0.64\omega$ rad	
$(C_{n_r})_W = -0.1$	$s_1 = 15.45$ ft		
$(C_{n_p})_W = -0.106$	$x_0 = 24$ ft		

The power spectral densities of yawing moment, rolling moment, and side force due to v_g are given by

$$\Phi_{N(v_g)} = |(N/v_g)_{FT}|^2\Phi_{v_g} \quad (40)$$

$$\Phi_{L(v_g)} = |(L/v_g)_{WT}|^2\Phi_{v_g} \quad (41)$$

$$\Phi_{Y(v_g)} = |(Y/v_g)_{FT}|^2\Phi_{v_g} \quad (42)$$

Equations (40–42) were evaluated for discrete values of frequency ω and are shown plotted in Figs. 4–6. The curves are normalized by the mean square values of gust velocity as given in the turbulence models of Eqs. (18) and (19). Likewise, Eqs. (22–25) were evaluated and plotted on the same figures.

The dotted curves in Figs. 4–6 are the power spectra of gust-induced yawing moment, rolling moment, and side force with uniform spanwise and axial distribution of gust velocities. Uniform u_g and w_g across the span will produce no yawing or rolling moments, and v_g uniform axially means lateral gust penetration effects are not included. With uniform dis-

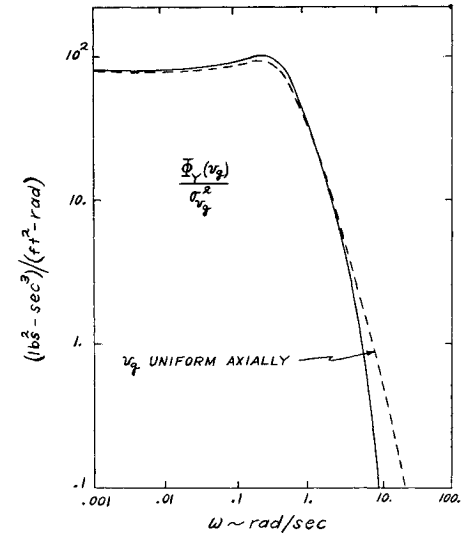

Fig. 6 Side force power spectra.

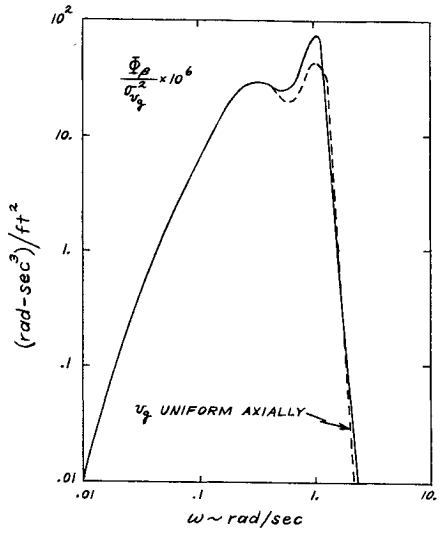

Fig. 7 Sideslip angle power spectra.

tributions, in terms of total-aircraft derivatives,

$$Y = \tfrac{1}{2}\rho U_0 S C_{y_\beta} v_g \quad (43)$$

$$N = \tfrac{1}{2}\rho U_0 S b C_{n_\beta} v_g \quad (44)$$

$$L = \tfrac{1}{2}\rho U_0 S b C_{l_\beta} v_g \quad (45)$$

And the power spectra are

$$\Phi_{Y(v_g)} = \left|\tfrac{1}{2}\rho U_0 S C_{y_\beta}\right|^2 \Phi_{v_g} \quad (46)$$

$$\Phi_{N(v_g)} = \left|\tfrac{1}{2}\rho U_0 S b C_{n_\beta}\right|^2 \Phi_{v_g} \quad (47)$$

$$\Phi_{L(v_g)} = \left|\tfrac{1}{2}\rho U_0 S b C_{l_\beta}\right|^2 \Phi_{v_g} \quad (48)$$

Examination of Fig. 4 shows that yawing moment due to u_g is an order of magnitude less than that due to w_g, which is in turn two to three orders of magnitude less than that due to v_g. Also, comparison of the two $\Phi_{N(v_g)}$ spectra shows penetration effects on yawing moment to be quite significant. The areas under the two curves indicate that the rms value of v_g-induced yawing moment is 73 σ_{v_g} with penetration effects included and 33 σ_{v_g} without.

Similarly, Fig. 5 indicates that rolling moment due to u_g and w_g are several orders of magnitude less and one order less, respectively, than that due to v_g. Comparison of the two $\Phi_L(v_g)$ power spectra with and without penetration effects included shows penetration effects on rolling moment to be negligible since the curves are nearly coincident below a frequency of 5 rad/sec. The contributions to the rolling moment of the portions of the spectra above 5 rad/sec are negligible.

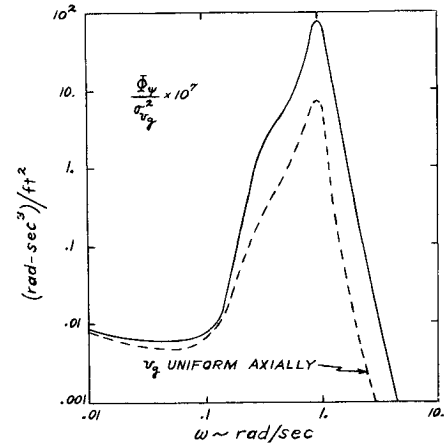

Fig. 8 Yaw angle power spectra.

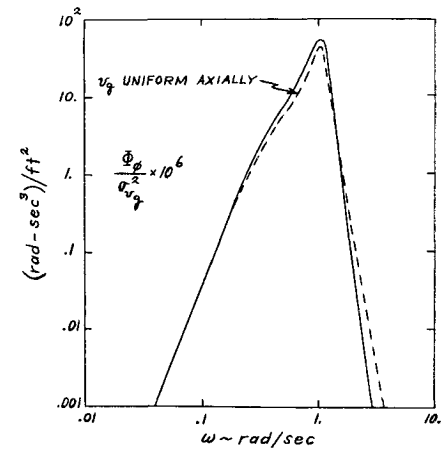

Fig. 9 Roll angle power spectra.

There is no contribution to side force from u_g and w_g; the contribution from v_g is shown in Fig. 6. Again, a comparison of the two $\Phi_Y(v_g)$ power spectra shows penetration effects to be negligible in determining the side force power spectral density.

The order-of-magnitude differences between the yawing moment, rolling moment, and side force power spectra due to u_g and w_g spanwise effects and the power spectra due to v_g allow the significant conclusion that spanwise variations in u_g and w_g are negligible in determining the lateral-directional responses of hovering VTOL aircraft and the gust-induced forces and moments acting thereon. Even wide variations in configuration parameters for various VTOL aircraft will not significantly alter the order-of-magnitude relationships shown previously. However, let it be emphasized again that these conclusions are drawn from an analysis based on linear aerodynamic theory, which in turn says that the gust forces and moments are due to circulation lift and not momentum transfer of energy from the gusts to the vehicle. For hover with low trim angles of attack and/or sideslip angles in less than severe turbulence (v_g/U_0 and w_g/U_0 less than about 6/25), circulation lift is the predominant mechanism.

Not a general conclusion, but for the VJ-101 analyzed, axial penetration of the lateral gusts, referenced at the center of gravity, is significant only for yawing moments and has a negligible effect in determining rolling moment and side force power spectra for the hovering aircraft.

Lateral-Directional Response

Now that we have established that only the lateral component of gust velocity need be considered in analyzing the lateral-directional response of the hovering aircraft, matrix equation (4) reduces to the following three equations for the sideslip, yaw, and roll response angles:

$$\beta = \left[\left(\frac{\beta}{Y}\right)\left(\frac{Y}{v_g}\right)_{FT} + \left(\frac{\beta}{N}\right)\left(\frac{N}{v_g}\right)_{FT} + \left(\frac{\beta}{L}\right)\left(\frac{L}{v_g}\right)_{WT}\right] v_g \quad (49)$$

$$\psi = \left[\left(\frac{\psi}{Y}\right)\left(\frac{Y}{v_g}\right)_{FT} + \left(\frac{\psi}{N}\right)\left(\frac{N}{v_g}\right)_{FT} + \left(\frac{\psi}{L}\right)\left(\frac{L}{v_g}\right)_{WT}\right] v_g \quad (50)$$

$$\phi = \left[\left(\frac{\phi}{Y}\right)\left(\frac{Y}{v_g}\right)_{FT} + \left(\frac{\phi}{N}\right)\left(\frac{N}{v_g}\right)_{FT} + \left(\frac{\phi}{L}\right)\left(\frac{L}{v_g}\right)_{WT}\right] v_g \quad (51)$$

In power spectral density form,

$$\Phi_\beta = \left|\left(\frac{\beta}{Y}\right)\left(\frac{Y}{v_g}\right)_{FT} + \left(\frac{\beta}{N}\right)\left(\frac{N}{v_g}\right)_{FT} + \left(\frac{\beta}{L}\right)\left(\frac{L}{v_g}\right)_{WT}\right|^2 \Phi_{v_g} \quad (52)$$

$$\Phi_\psi = \left|\left(\frac{\psi}{Y}\right)\left(\frac{Y}{v_g}\right)_{FT} + \left(\frac{\psi}{N}\right)\left(\frac{N}{v_g}\right)_{FT} + \left(\frac{\psi}{L}\right)\left(\frac{L}{v_g}\right)_{WT}\right|^2 \Phi_{v_g} \tag{53}$$

$$\Phi_\varphi = \left|\left(\frac{\phi}{Y}\right)\left(\frac{Y}{v_g}\right)_{FT} + \left(\frac{\phi}{N}\right)\left(\frac{N}{v_g}\right)_{FT} + \left(\frac{\phi}{L}\right)\left(\frac{L}{v_g}\right)_{WT}\right|^2 \Phi_{v_g} \tag{54}$$

Equations (52–54) were evaluated for discrete values of frequency, normalized by the variance or mean square value of v_g, and plotted as the solid curves in Figs. 7–9. These curves include penetration effects, and $(N/v_g)_{FT}$, $(Y/v_g)_{FT}$, and $(L/v_g)_{WT}$ in Eqs. (52–54) are as given in Eqs. (30, 31, and 39). The dotted curves in these figures give the response power spectra without lateral gust penetration effects included, and were derived from Eqs. (52–54) with the following terms, obtained from Eqs. (43–45), used in place of the frequency-dependent gust transfer functions:

$$(Y/v_g) = \tfrac{1}{2}\rho U_0 S C_{y\beta} \tag{55}$$

$$(N/v_g) = \tfrac{1}{2}\rho U_0 S b C_{n\beta} \tag{56}$$

$$(L/v_g) = \tfrac{1}{2}\rho U_0 S b C_{l\beta} \tag{57}$$

Study of Figs. 7–9 reveals that differences in the response spectra are most pronounced near the closed-loop dutch-roll frequency of l. rad/sec. The mean-square values of β, ψ, and ϕ were obtained by graphically integrating Eqs. (8–10), both with and without (v_g uniform axially) lateral gust penetration effects included. With penetration effects:

$$\sigma_\beta^2 = 1.492 \times 10^{-4}\sigma_{v_g}^2 \qquad \sigma_\psi^2 = 12.955 \times 10^{-6}\sigma_{v_g}^2$$

$$\sigma_\phi^2 = 91.17 \times 10^{-6}\sigma_{v_g}^2 \qquad \sigma_\beta = 1.222 \times 10^{-2}\sigma_{v_g}$$

$$\sigma_\psi = 3.6 \times 10^{-3}\sigma_{v_g} \qquad \sigma_\phi = 9.57 \times 10^{-3}\sigma_{v_g}$$

Without penetration effects:

$$\sigma_\beta^2 = 53.1 \times 10^{-6}\sigma_{v_g}^2 \qquad \sigma_\psi^2 = 1.014 \times 10^{-6}\sigma_{v_g}^2$$

$$\sigma_\phi^2 = 73.38 \times 10^{-6}\sigma_{v_g}^2 \qquad \sigma_\beta = 7.3 \times 10^{-3}\sigma_{v_g}$$

$$\sigma_\psi = 1.008 \times 10^{-3}\sigma_{v_g} \qquad \sigma_\phi = 8.58 \times 10^{-3}\sigma_{v_g}$$

The ratios of rms response with penetration to rms response without penetration effects are

σ_β ratio = 1.67 σ_ψ ratio = 3.57 σ_ϕ ratio = 1.12

Thus, on this particular vehicle with the assumed stability augmentation, neglect of penetration effects gives unconservative results for all three response angles.

For a lateral gust intensity (rms value σ_{v_g}) of 6 fps, the rms responses with penetration effects included are: $\sigma_\beta = 4.20°$; $\sigma_\psi = 1.24°$; $\sigma_\phi = 3.29°$. Without penetration effects included: $\sigma_\beta = 2.51°$; $\sigma_\psi = 0.35°$; $\sigma_\phi = 2.95°$.

Conclusions and Recommendations

1) The linear aerodynamic theory used herein is reasonably accurate (about 10% error) for summed trim and gust-induced angles of attack and sideslip angles up to the limit of lift curve slope linearity. For larger trim and gust input angles an approach based on momentum transfer of gust energy to the aircraft should be developed and applied.

2) In the linear aerodynamic range, spanwise variations of longitudinal and vertical components of gust velocity are negligible in determining gust-induced side force, yawing moment, rolling moment, and sideslip, yaw, and roll power spectra and rms response angles for hovering VTOL aircraft. Only the lateral gust velocity component need be considered; and, in general, the axial distribution or penetration effects must be accounted for. The longitudinal dynamics were not considered in this work; however, it seems reasonable that spanwise distributions of u_g and w_g would have even less effect on pitch angle response than they have on roll and yaw response. On the other hand, axial distribution of w_g (penetration effect) would appear to be as significant to pitch response as axial distribution of v_g is to lateral-directional response. It is recommended that these effects on longitudinal response be investigated. The analytical methods herein and in the mentioned references are directly applicable to the longitudinal case.

3) The power spectra of β, ψ, and ϕ peak in the vicinity of the closed-loop dutch-roll natural frequency (1 rad/sec in the example presented), and the differences in the spectra with and without v_g penetration effects are greatest there. Thus, great care should be exercised in calculating the spectra in this region.

4) The analysis methods outlined in this work should be applied to VTOL aircraft in various stages of transition flight to determine the range of flight conditions where spanwise effects of u_g and w_g are no longer negligible compared to v_g effects.

References

[1] Etkin, B., "A Theory of the Response of Airplanes to Random Atmospheric Turbulence," *Journal of the Aero/Space Sciences*, Vol. 26, 1959, pp. 409–420.

[2] Eggleston, J. M. and Phillips, W. H., "The Lateral Response of Airplanes to Random Atmospheric Turbulence," TR R-74, pp. 41–52, 1960, NASA.

[3] *Dynamics of the Airframe*, Rept. AE-61-4II, Chap. II, 1952, Bureau of Aeronautics, Dept. of the Navy.

[4] Eggleston, J. M. and Diederich, F. W., "Theoretical Calculation of the Power Spectra of the Rolling and Yawing Moments on a Wing in Random Turbulence," Rept. 1321, 1957, NACA.

[5] Eggleston, J. M., "Calculations of the Forces and Moments on a Slender Fuselage and Vertical Fin Penetrating Lateral Gusts," TN 3805, 1956, NACA.